Gold-Hyperdoped Black Silicon With High IR Absorption by Femtosecond Laser Irradiation

Xin-Yue Yu, Ji-Hong Zhao, *Member, IEEE*, Chun-Hao Li, Qi-Dai Chen, and Hong-Bo Sun, *Member, IEEE*

***Abstract*—Gold (Au)-doped-textured silicon (Si) material with a thermostable absorption below bandgap (>50%) is obtained by femtosecond laser irradiation. Although the concentration of Au impurity (10^{19} cm^{-3}) in textured Si is at least four orders of magnitude greater than the solid solubility of Au in crystalline Si, the sheet carrier density (approximately 10^{10} cm^{-2}) in Au-doped Si is very low due to a self-compensation effect of Au impurity in Si material. The infrared absorption of Au-doped Si is related to laser-induced-structural defects and sub-band absorption of deep energy levels of Au in Si, which is determined by temperature-dependent Hall Effect measurement. Besides supersaturated doping of Au, a gold silicide phase is formed at textured Si surface.**

***Index Terms*—Black silicon, femtosecond laser, gold, hyperdoping, infrared absorption.**

I. Introduction

SILICON (Si) materials hold the naturally dominant position in producing Si based optoelectronic integrated devices like photodetectors owing to its low-cost and the excellent compatibility with modern complementary metal-oxide semiconductor (CMOS) technology. However the application in infrared photodetection is principally restricted by its 1.12 eV bandgap. In recent years, to extend the absorption wavelength, studies on supersaturated Si with chalcogens (sulfur, selenium, and tellurium) fabricated using femtosecond (fs) laser ablation and ion implantation followed by pulsed laser melting have attracted more attention of researchers [1]–[5], [26]–[29]. The most concentrated interest of hyperdoped Si with chalcogens is in their high absorptance for photons with energy below the bandgap of crystalline Si. For example, the absorptance in infrared region (1.1∼2.5 μm) of fs laser irradiated black Si microstructure with chalcogen dopants is up to 90% [2]. The distinct property of high infrared absorption makes this black Si material a better candidate for applications in infrared photodetection fields [6]–[8]. Unfortunately, the infrared absorption contributions of sulfur (S)-doped black Si include a quite large proportion of free carrier absorption which is bad for infrared detection applications due to a large background noise [9]. What is worse, the infrared absorptance of S-doped Si is unstable and drops seriously after thermal annealing at temperature as low as 825 K (about 20%) [4]. To overcome the above two weakness of S-doped Si (high free carrier absorption and instability of infrared absorption), transition metal element gold (Au)-hyperdoped Si by fs laser is a good choice. Firstly, supersaturated Au impurity can introduce deep energy levels or even form an impurity band in the bandgap of Si and cause sub-band absorption [10]. Furthermore, Au-doped Si will lower the free carrier absorption contribution due to self-compensation effect of Au impurities in Si [11]. Last but not least, all the absorption of fs laser textured Si will be enhanced by multiple reflections of geometric microstructures during a complex interaction process between laser and material [12], [13]. Accordingly, in this paper the supersaturated Au-doped Si using fs laser irradiation has been prepared and a high thermostable infrared absorption has been observed. This report provides a powerful support for the infrared detection application of the fs laser irradiated Si.

II. Experiments

The double-polished, nearly-intrinsic Si (111) wafer (n-type, 1500 Ω • cm resistivity, 260 μm thickness) was treated by standard cleaning procedures [14]. The cleaned Si surface was covered by 40 nm thick Au film that was coated by vacuum thermal evaporation technique and then was transformed into a vacuum chamber which can be fixed in a three-dimensional (3D) translation stage. In order to fabricate Au-doped black Si the air in the chamber was evacuated firstly and then filled by Argon (Ar) atmosphere of 0.16 MPa. Further, the Au-covered Si substrate was irradiated by a Ti: sapphire fs laser amplifier (Spectra-Physics) with 100 fs pulse duration, 800 nm center wavelength, and 2.5 kHz repetition rate. Using a long focus lens of 600 mm focal distance the fs laser spot was focused to 260 μm-diameters and irradiated onto the front surface of Si which was covered by the Au film. The S-line sweep speed was 1 mm/s and the interval of the scanning line was designed to be 30 μm. The schematic diagram of fs laser fabrication system is shown in Fig. 1. The optical properties of Au-doped black Si and Si substrate are measured by a spectrophotometer (Shimadzu UV-3600) equipped with an integrating sphere (LISR-UV3100). With the spectrophotometer, we measure the total hemispherical (specular and diffuse) reflectance (R) and transmittance (T) of a sample. By measuring both the reflectance and transmittance from 0.25 to 2.5 μm, we calculate the absorptance (A) of each sample with A = 1-R-T.

Manuscript received March 8, 2017; revised March 27, 2017; accepted April 10, 2017. Date of publication April 12, 2017; date of current version May 8, 2017. This work was supported by the National Natural Science Foundation of China (NSFC) under Grants #61235004, # 61307119, # 61590930, # 61377048, and # 61378053. The review of this paper was arranged by Associate Editor X. Zhang. *(Corresponding author: Ji-Hong Zhao.)*

The authors are with the State Key Laboratory on Integrated Optoelectronics, College of Electronic Science and Engineering, Jilin University, Changchun 130012, China (e-mail: zhaojihong@jlu.edu.cn).

Color versions of one or more of the figures in this paper are available online at http://ieeexplore.ieee.org.

Digital Object Identifier 10.1109/TNANO.2017.2693691

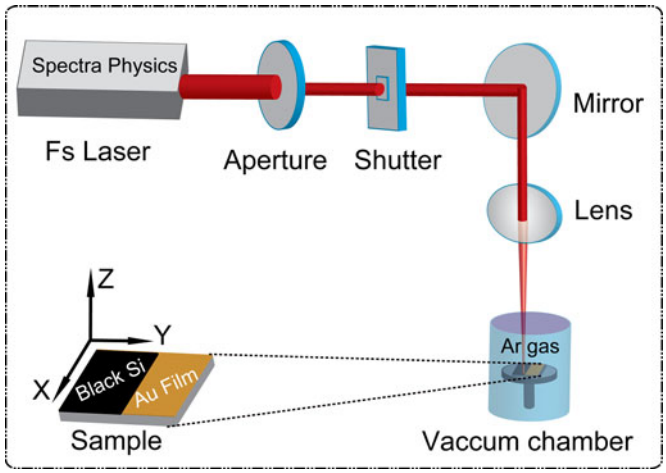

Fig. 1. The schematic diagram of fs laser fabrication system.

Here the absorptance is defined as $\Phi^a_{e,\lambda}/\Phi^i_{e,\lambda}$, where $\Phi^a_{e,\lambda}$ is the spectral radiant flux in wavelength absorbed by that surface, and $\Phi^i_{e,\lambda}$ is the spectral radiant flux in wavelength received by that surface. The surface morphology images are obtained using a field emission scanning electron microscope (SEM, JSM-7500F, JEOL, and Japan). To investigate the structures of Au-doped Si, X-ray photoelectron spectroscopy (XPS) was performed using an ESCALAB 250 spectrometer. The atomic concentrations of Au in the Si substrate before and after the annealing were analyzed by secondary ion mass spectrometry (SIMS). This instrument is equipped with a CAMECA 4F device using a 14.5 keV acceleration voltage at an incident angle of 30 degrees from the surface normal. Finally, the electrical properties were obtained by an ACCENT HL5500PC Hall system and temperatures of samples can be changed from the temperature of liquid nitrogen to room temperature.

III. Results and Discussion

The Au-doped black Si samples (S) are fabricated using four laser powers (S1∼S4): 100, 200, 300, and 400 mW, respectively. The surface morphologies of S1∼S4 are shown in Fig. 2(a)–(d). From Fig. 2 we can find that the bead-like microstructures appear in Si surface after fs laser irradiation with low laser power (below 200 mW). Then these microstructures grow up to spike shape for higher laser powers (above 300 mW). The size of microstructures increases with the increasing of the laser power while the densities per unit area of microstructures decrease. The observed heights of microstructures should be multiplied by 1.41 because there is a tilt angle of 45° in SEM images measurement. Then, the real heights of microstructures of S1∼S4 approximately are 2.2 μm, 2.3 μm, 9.2 μm, and 15.5 μm, respectively. However, the periods of microstructures are not dramatically changed for four samples, which vary from 1.7 μm to 5.5 μm. The absorptance at wavelengths of 0.25∼2.5 μm of Au-doped unannealed Si and corresponding annealed samples is shown in Fig. 2(e). Compared with the absorptance of flat Si substrate, the absorptance of all the investigated samples is enhanced at the whole wavelength range. Here the increase

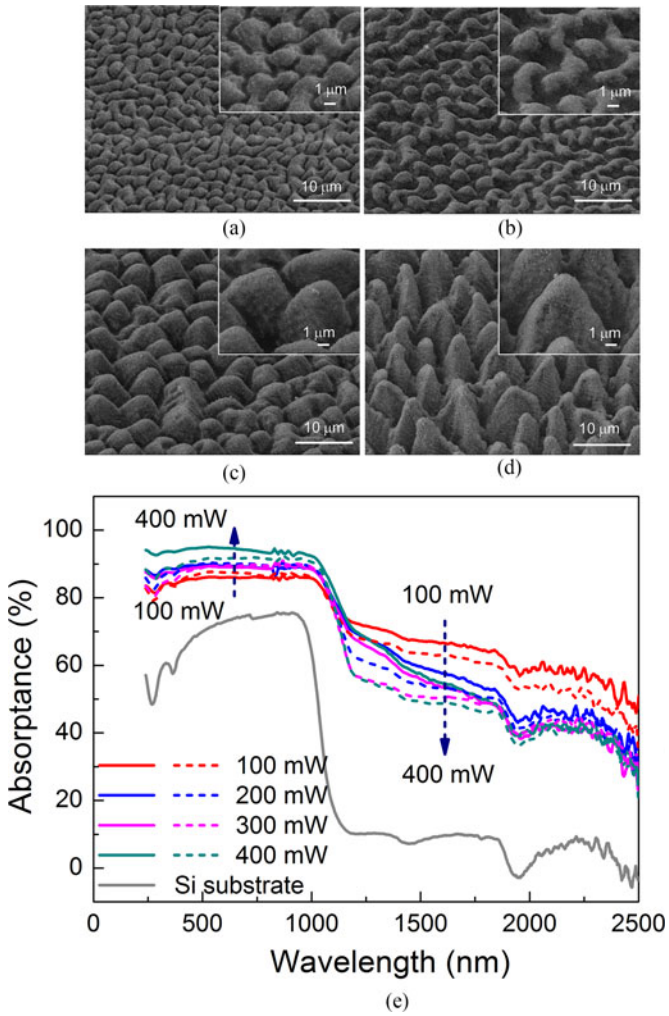

Fig. 2. (a)–(d) SEM images (tilt 45°) of Au-doped black Si fabricated by fs laser at different laser powers: (a) 100, (b) 200, (c) 300, (d) 400 mW. Insets are partial enlarged view of main pictures. (e) The absorptance of S1∼S4 before (straight lines) and after annealing (shot dish lines) at 823 K for 30 min. The absorptance of flat silicon substrate also is performed. In addition, annealing process will not affect the absorptance of flat silicon substrate.

of absorptance above bandgap of Si (0.25–1.1 μm) can be attributed to multiple reflections from geometric microstructures [25] and absorption increases with laser power in Fig. 2(e). Traditionally, the enhancement of absorptance below bandgap of Si ($\lambda = 1.1\sim2.5$ μm) can be speculated to be a combination of sub-band absorption from Au impurity levels and Urbach state absorption from structural defects induced by fs laser ablation [15], [16]. For the absorption contribution from structural defects, the decreasing variation tendency of absorptance with wavelength reflects the existence of structural defects related to the amorphous Si (α-Si) phase in fs laser ablated region which can be observed in Raman spectra of Au-doped Si samples [14]. Furthermore, for the sub-band absorption contribution from Au doping can be confirmed by comparing absorption with the concentration distribution of Au impurities. For fs laser irradiated Si under vacuum, the infrared absorption can be enhanced by the multiple reflections effects of geometry and the infrared absorptance increases with the increasing of size of microstructures (or

ablation power) [14]. Contrarily, for Au-doped Si, the absorptance below bandgap (1.1∼2.5 μm) decreases with an increasing laser power. The drop in infrared absorption with laser power is observed in Fig. 2(e), suggesting a significant contribution from Au-induced impurity levels and sub-bandgap absorption at lower laser powers. There will be higher Au atomic concentration due to a weak damage to Au film from laser ablation at lower laser powers.

Fig. 2(e) also shows that the absorption below bandgap of all Au-doped Si decreases after a thermal treatment in argon atmosphere (823 K and 30 min). The largest reduction of absorptance below bandgap in all samples does not exceed 15%. Specifically, the absorptance at wavelengths of 1.1∼1.8 μm sharply drops due to the fact that the majority of thermally sensitive structural defects related to Urbach states eliminated (partial crystallization of α-Si phase). However, the effect of thermal treatment on absorptance at wavelengths of 1.8∼2.5 μm is more obvious for the samples obtained at lower laser powers because of that at this region the absorption contribution mainly comes from sub-band absorption of deep levels of Au impurity. At the lower laser powers where there is the possibility of Au-induced impurity levels and absorption from supersaturated Au in Si, thermal annealing will cause Au to come out of solution (precipitate) and lower the sub-bandgap absorption. However at higher laser powers where Au may be completely ablated, the thermal effect may well be to reduce Si defects, and recrystallization of amorphous Si, and these effects can decrease absorption as observed.

To clarify the structural nature of fs laser-textured Si, the chemical states of Au and Si atoms of annealed samples (823 K and 30 min) are investigated by XPS. The correction of the XPS spectra for the charge accumulation is performed using C 1 s peak (Binding Energy (BE) = 284.6 eV). Here $\boldsymbol{s} = 0$, $\boldsymbol{p} = 1$, $\boldsymbol{f} = 3$, represent electronic orbit levels.

Fig. 3(a) shows XPS spectra of Au 4*f* lines obtained for the S1 sample. The peaks of Au $4f_{7/2}$ and Au $4f_{5/2}$ (spin-orbit components) lines are located at BE = 85.2 and 88.9 eV. An Au $4f_{7/2}$ peak appeared at 85.2 eV corresponds to the gold in silicide phase [21]. Fig. 3(b) shows XPS spectra of Si 2p system of S1 sample. The peak is deconvoluted to peaks at 101.77eV and 102.7 eV. The nature of Si 2*p* line may be due to the formation of several chemical states of Si–Au or Si–O or Au–Si–O [22]. Therefore, it is clear that the gold silicide (Au–Si) eutectic composition is formed in Au-doped Si surface.

To measure the distribution level of Au impurities in the resolidified Si layer after fs laser irradiation the concentration distribution of Au impurities in the uppermost 1 μm of black Si surface after irradiation of 100 mW laser power (S1), which has smallest surface roughness in all samples, is measured by SIMS. The spectrum in Fig. 4 is obtained by sputtering the sample surface with Cs^+ while performing a secondary ion mass spectrometer scan. The impurity concentration is measured in a circular surface area of 200 μm diameter (containing hundreds microstructures) along the textured Si substrate, so the SIMS data reflects an average distribution of Au impurities in the detected area. Considering the effect of microstructures on actual measurement, the depth in Fig. 4 is effective depth, which has been corrected by calculation model of depth [24]. According

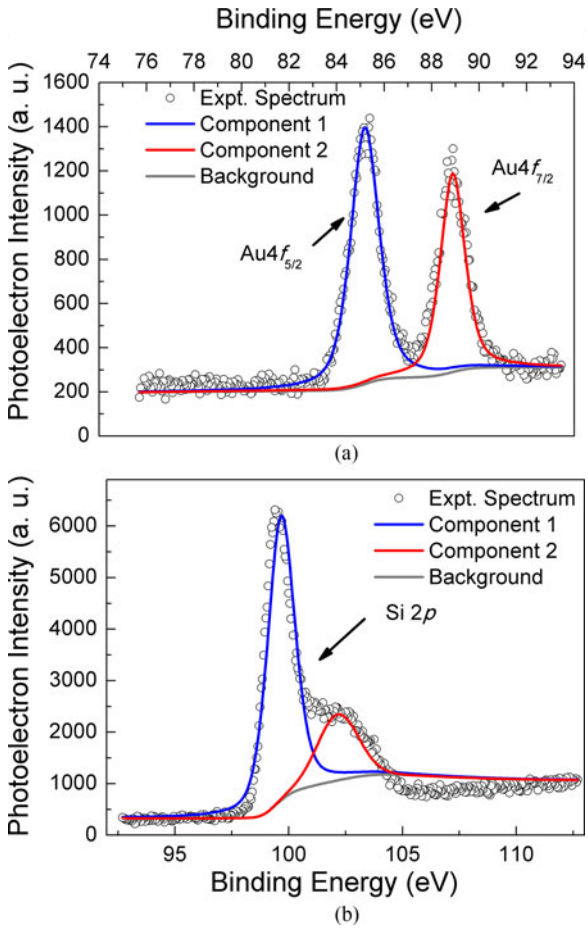

Fig. 3. XPS spectra of Au-doped Si sample fabricated with 100 mW laser power (S1): (a) Au 4*f* system and (b) Si 2*p* system. Gray lines in (a) and (b) are background.

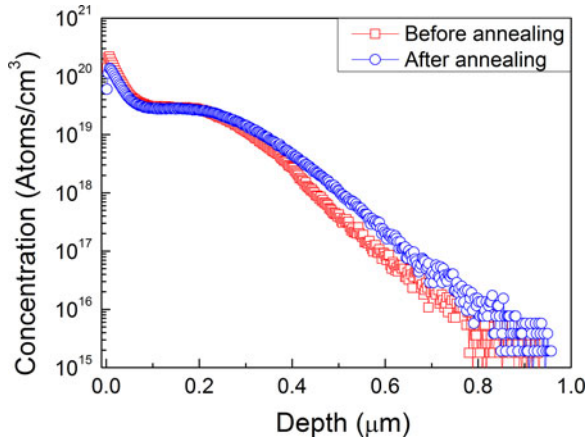

Fig. 4. SIMS depth profiles of Au in fs laser irradiated Si (S1) and corresponding thermal annealed Sample (823 K and 30 min at Ar atmosphere).

to Fig. 4, the average Au impurity concentration in the uppermost 25 nm is about 10^{20} atom/cm^3 and then decreases with the increasing of detecting depth. It is worth noting that in the depth of 100∼250 nm the Au concentration is stabilized around 2.5×10^{19} atom/cm^3, several orders of magnitude above the solid solubility of Au atoms in Si crystals (The solid solubility

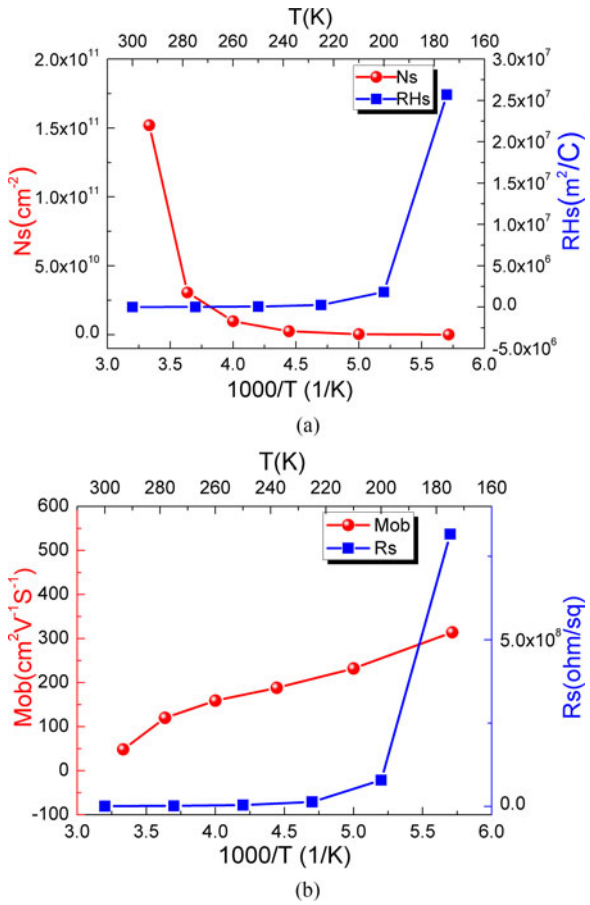

Fig. 5. (a) The temperature dependency of sheet carrier density and Hall coefficient of annealed Au-doped Si sample (S1); (b) The temperature dependency of mobility and square resistance of S1 sample.

limit of Au in Si at room temperature is estimated to be below 10^{15} atoms/cm^3) [18], [19]. The Au concentration remains nearly the same order of magnitude in black Si layer after thermal annealing treatment (823 K and 30 min) and the obvious diffusion of Au impurities into Si bulk from surface can be observed in SIMS curve after thermal annealing process.

Finally, the electronic nature of Au-doped layer is determined by Hall-Effect measurement based on the van der Pauw technique [23]. The sheet carrier density of annealed Au-doped samples varies in the range of $2.66 \times 10^{10} \sim 5.73 \times 10^{10}$ cm^{-2} for four annealed samples (823 K and 30 min), which near 3.26×10^{10} cm^{-2} of the carrier density of high resistant Si substrate at room temperature. Such low carrier density is a result of self-compensation effect of deep donor level ($E_v + 0.35$ eV) and deep acceptor level ($E_c - 0.54$ eV) of Au impurity [10], where E_v and E_c are the edge of valence-band and conduction-band, respectively. At room temperature the conductive type of annealed S1 is p-type, however, others three annealed samples (S2$\sim$S4) show n-type. Furthermore, the temperature dependent-Hall Effect is measured and electric parameters of Au-doped Si are described in Fig. 5. Fig. 5(a) shows the variation of sheet carrier density and Hall coefficient of annealed Au-doped Si (S1-823K and 30 min) with temperature (175 K to 300 K). The sign of Hall coefficient is positive and the sheet carrier density

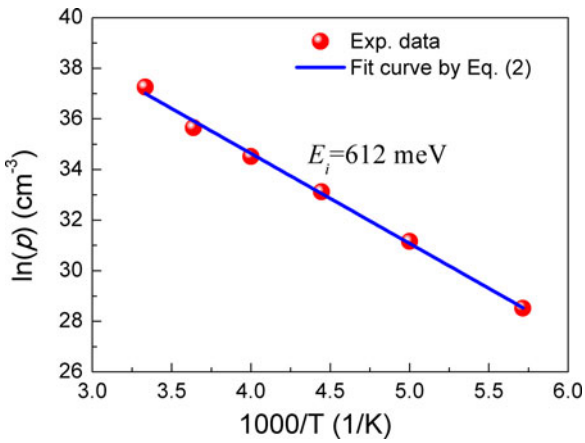

Fig. 6. Temperature-dependent concentration p of carrier's holes of Au-doped Si sample S1.

increases with increasing temperature. Now, the conductive carriers are holes that may come from the acceptor energy level of Au impurity. In addition, increasing temperature will raise the carrier's concentration. Fig. 5(b) shows the dependence of carrier mobility and square resistance on temperature. With the increasing temperature, the carrier mobility decreases due to enhancing lattice scattering. Moreover the increasing carrier density will induce a decreasing square resistance in Fig. 5(b).

Temperature-dependent Hall Effect measurements can be applied to fit the energy level of Au impurity states in Si. In Fig. 5(a) the acceptor energy level of Au impurity should be dominant because the conductive carries are holes. If the degree of compensation is small in Au-doped Si such that it is possible for $N_d \ll p \ll N_a$, the carrier holes concentration p can be written as (1) [10].

$$p = (\beta N_v N_a)^{1/2} \exp(-E_i/2kT) \tag{1}$$

Where β is spin degeneracy, N_v is band edge density of states, N_d and N_a are the concentration of donor and acceptor impurity, respectively. E_i is the ionization energy of Au acceptor, T is the temperature, k is the Boltzmann constant. The concentration p of carrier holes in Eq. (1) can be transformed to the following form.

$$ln(p) \propto -(E_i/2k)/T \tag{2}$$

The concentration p of holes of Au-doped Si sample S1 can be obtained by N_S/d, N_S is the sheet carrier density [see Fig. 5(a)], d is the depth of Au doping layer, which can be determined by SIMS spectrum ($\sim$500 nm). According to the Eq. (2), a plot of ln(p) versus 1/T will exhibit a slope of $E_i/2k$. Fig. 6 shows the fitting results of holes concentration and the ionization energy of Au acceptor impurity is estimated to 612 meV. The fitted result is approximative to the ionization energy of Au acceptor impurity in crystalline Si ($\sim$580 meV) and this difference may be related to the complex structures in Au-doped Si surface.

IV. Conclusion

In conclusion, the supersaturated Au impurity has been doped into microstructured Si samples surface by fs laser ablation.

A concentration of 10^{19} atom/cm^3 of Au impurity in Si has been obtained by SIMS measurement. There is a high and thermostable absorptance below the bandgap in Au-doped Si. The larger absorptance below the bandgap is a result of combination of structural defect absorption and sub-band absorption of Au impurity in Si. All the absorption can be enhanced by the multi-reflections effect of geometric microstructures. XPS measurements determine that there is gold silicide in Au-doped Si surface. Another good performance of Au-doped Si is that the sheet carrier density is very low owing to the self-compensation effect between donor and acceptor levels of Au impurities in Si.

REFERENCES

[1] T. H. Her, R. J. Finlay, C. Wu, S. Deliwala, and E. Mazur, "Microstructuring of silicon with femtosecond laser pulses," *Appl. Phys. Lett.*, vol. 73, pp. 1673–1675, 1998.

[2] C. Wu *et al.*, "Near-unity below-bandgap absorption by microstructured silicon," *Appl. Phys. Lett.*, vol. 78, pp. 1850–1852, 2001.

[3] M. A. Sheehy, B. R. Tull, C. M. Friend, and E. Mazur, "Chalcogen doping of silicon via intense femtosecond-laser irradiation," *Mater. Sci. Eng. B*, vol. 137, pp. 289–294, 2006.

[4] B. R. Tull, M. T. Winkler, and E. Mazur, "The role of diffusion in broadband infrared absorption in chalcogen-doped silicon," *Appl. Phys. A*, vol. 96, pp. 327–334, 2009.

[5] M. Smith *et al.*, "Pressure-induced phase transformations during femtosecond-laser doping of silicon," *J. Appl. Phys.*, vol. 110, 2011, Art. No. 053524.

[6] Z. Huang, J. E. Carey, M. Liu, X. Guo, E. Mazur, and J. C. Campbell, "Microstructured silicon photodetector," *Appl. Phys. Lett.*, vol. 89, pp. 033506–033508, 2006.

[7] M. J. Sher, M. Winkler, and E. Mazur, "Pulsed-laser hyperdoping and surface texturing for photovoltaics," *MRS Bull.*, vol. 36, pp. 439–445, 2011.

[8] A. J. Said *et al.*, "Extended infrared photoresponse and gain in chalcogen-supersaturated silicon photodiodes," *Appl. Phys. Lett.* vol. 99, 2011, Art. No. 073503.

[9] J. T. Sullivan *et al.*, "Methodology for vetting heavily doped semiconductors for intermediate band photovoltaics: A case study in sulfur-hyperdoped silicon," *J. Appl. Phys.* vol. 114, 2013, Art. No. 103701.

[10] S. M. Sze and K. K. Ng, *Physics of Semiconductor Device*. New York, NY, USA: Wiley, 2006.

[11] J. P. Mailoa *et al.*, "Room-temperature sub-bandgap optoelectronic response of hyperdoped silicon," *Nature Commun.*, vol. 5, 2014, Art. No. 3011.

[12] K. A. Willets and R. P. Van Duyne, "Localized Surface Plasmon Resonance Spectroscopy and Sensing," *Annual Rev. Phys. Chem.*, vol. 58, pp. 267–297, 2007.

[13] X. B. Li, X. Q. Liu, X. D. Han, and S. B. Zhang, "Role of electronic excitation in phase change memory materials: A brief review," *Phys. Status Solidi B*, vol. 249, p. 1861, 2012.

[14] C. H. Li *et al.*, "Infrared absorption of femtosecond laser textured silicon under vacuum," *IEEE Photon. Technol. Lett.* vol. 27, no. 14, pp. 1481–1484, Jul. 15, 2015.

[15] A. Barhdadi, B. Hartiti, and J. C. Muller, "Active defects generated in silicon by laser doping process," *African Rev. Phys.* vol. 6, pp. 229–238, 2011.

[16] A. F. Banishev, V. S. Golubev, and A. Yu. Kremnev, "Effect of the ambient atmosphere and the gas type on generation of defects and destruction of silicon surface under the action of laser pulses," *Techni. Phys*., vol. 49, pp. 1035–1039, 2004.

[17] Y. Y. Wong, M. Yahaya, M. M. Salleh, and B. Y. Majlis, "Controlled growth of silicon nanowires synthesized via solid-liquid-solid mechanism," *Sci. Technol. Adv. Mater.* vol. 6, pp. 330–334, 2005.

[18] F. A. Trumbore, "Solid solubilities of impurity elements in germanium and silicon," *Bell Syst. Tech. J.*, vol. 39, pp. 205–233, 1960.

[19] S. F. Cagnina, "Enhanced gold solubility effect in heavily n-type silicon," *J. Electrochem. Soc*. vol. 116, pp. 498–502, 1969.

[20] E. D. Diebold, N. H. Mack, S. K. Doorn, and E. Mazur, "Femtosecond laser-nanostructured substrates for surface-enhanced Raman scattering," *Langmuir*, vol. 25, pp. 1790–1794, 2009.

[21] B. Sundaravel *et al.*, "XPS and SIMS analysis of gold silicide grown on a bromine passivated Si(111) substrate," *Appl. Surface Sci.*, vol. 137, pp. 103–112, 1999.

[22] D. K. Sarkar *et al.*, "XPS studies on silicide formation in ion beam irradiated Au/Si system," *Appl. Surface Sci.*, vol. 120, pp. 159–164, 1997.

[23] C. H. Li *et al.*, "Fabrication of black silicon with thermostable infrared absorption by femtosecond laser," *IEEE Photon. J.* vol. 8, no. 6, Dec. 2016, Art. No. 6805809.

[24] X. Dong *et al.*, "A nitrogen-hyperdoped silicon material formed by femtosecond laser irradiation," *Appl. Phys. Lett.* vol. 104, 2014, Art. No. 091907.

[25] M. J. Sher *et al.*, "Mid-infrared absorptance of silicon hyperdoped with chalcogen via fs-laser irradiation," *J. Appl. Phys.*, vol. 113, 2013, Art. No. 063520.

[26] S. Höhm, M. Herzlieb, A. Rosenfeld, J. Krüger, and J. Bonse, "Femtosecond laser-induced periodic surface structures on silicon upon polarization controlled two-color double-pulse irradiation," *Opt. Exp.*, vol. 23, pp. 61–71, 2015.

[27] X. Y. Yu, Z. H. Lv, C. H. Li, X. Han, and J. H. Zhao, "The optical and electrical properties of co-doped black silicon textured by a femtosecond laser and its application to infrared light sensing," *IEEE Sens. J.*, vol. 16, no. 13, pp. 5227–5231, Jul. 1, 2016.

[28] C. H. Lai *et al.*, "Gold-nanoparticle coated silicon cone array for surface-enhanced Raman spectroscopy," *Spectrosc. Lett.*, vol. 49, pp. 51–55, 2016.

[29] X. S. Zhang, F. Y. Zhu, G. Y. Sun, and H. X. Zhang, "Fabrication and characterizations of squama-shape micro/nano multi-scale silicon material," *Sci. China Technol. Sci.*, vol. 55, pp. 3395–3400, 2012.

Authors' photographs and biographies not available at the time of publication.